Tutorial: Novel properties of defects in semiconductors revealed by their vibrational spectra

Michael Stavola[a] and W. Beall Fowler
Department of Physics, Lehigh University, Bethlehem, Pennsylvania 18015, USA

(Received 29 October 2017; accepted 13 December 2017; published online 10 January 2018)

This is an introductory survey of the vibrational spectroscopy of defects in semiconductors that contain light-mass elements. The capabilities of vibrational spectroscopy for the identification of defects, the determination of their microscopic structures, and their dynamics are illustrated by a few examples. Several additional examples are discussed, with a focus on defects with properties not obviously accessible by vibrational spectroscopy, such as the diffusivity of an impurity, the negative U ordering of electronic levels, and the time constant for a nuclear-spin flip. These novel properties have, nonetheless, been revealed by vibrational spectra and their interpretation by theory. *Published by AIP Publishing.* https://doi.org/10.1063/1.5011036

I. INTRODUCTION

Spectroscopies of various kinds have been used for decades to reveal the microscopic properties of defects and impurities in semiconductors.[1–3] Because of the critical role spectroscopies and their interpretation by theory have played for understanding defects, they have been central themes of the International Conference on Defects in Semiconductors (ICDS) since the first ICDS that was held in Gatlinburg, Tennessee, May 1959.[4]

The light-mass elements such as H, Li, B, C, N, O, and Si are among the most common elements in nature and are, therefore, the most common contaminants that are introduced into semiconductors during crystal growth and device processing.[2,5] The light elements can also be introduced intentionally to exploit their beneficial effects on materials properties. Whether introduced accidentally or by design, the light-mass elements in semiconductors must be thoroughly understood so that device materials can be reproducibly engineered. Vibrational spectroscopy has proved to be an essential probe of the light-mass elements and is the focus of this tutorial.[5–12]

In the present paper, the fundamentals of vibrational spectroscopy and a selection of the defects that have been studied by this method are surveyed. A few examples have been chosen to illustrate the power of vibrational spectroscopy for the identification of defects and the determination of their structures. Other examples illustrate the situations where the novel properties of defects have been revealed by their vibrational spectra.

In a brief tutorial about a field with a long history, it is not possible to be comprehensive. Fortunately, several excellent reviews have been written about advancements in the vibrational spectroscopy of defects and impurities in semiconductors, which summarize and cite the extensive literature in this important sub-field of defect study.[5–12]

II. LOCAL VIBRATIONAL MODES

The addition to a host crystal of an impurity atom whose mass is lighter than the masses of the host atoms gives rise to new vibrational modes with higher frequencies than the host crystal's vibrational modes. The vibrational properties of a light-mass impurity are well illustrated by simple models. Consider a linear monatomic chain of atoms connected by bonds with equal force constants as a model for the phonons in an elemental host crystal. If one of the host atoms is replaced by an impurity with a lighter mass, a new vibrational mode emerges at higher frequency from the host crystal's vibrational spectrum.[5–11] Because of their larger masses, the heavier host atoms cannot follow the vibrations of the light impurity. The high-frequency vibrational mode cannot propagate in the crystal, and only the light impurity atom and its nearest neighbors vibrate appreciably. Because this impurity mode is spatially localized, it is referred to as a localized vibrational mode (LVM).

There can also be resonant vibrational modes with sharp spectral frequencies that lie in regions where the density of host phonon modes is small. For compound semiconductors, there can also be vibrational modes that lie between the acoustic and optic phonon branches, referred to as gap modes. However, most studies are concerned with LVMs that occur in the high-frequency spectral range above the maximum phonon frequency, where the host crystal is transparent.

A. Infrared and Raman spectroscopies

The LVMs of impurities can be studied by infrared (IR) absorption[5–11] or by Raman[13] spectroscopies. While IR spectroscopy is the method more commonly used to study the LVMs of impurities, in some cases Raman measurements provide important complementary information or are better matched to the characteristics of the particular sample or defect being studied.

1. Infrared spectroscopy

In IR absorption experiments, the transmission vs. frequency for a sample containing a defect of interest is measured. The transmission, T, is given by[8,14]

[a]michael.stavola@Lehigh.edu

$$T = \frac{I}{I_0} = \frac{(1-R)^2\, e^{-\alpha x}}{(1-R^2\, e^{-2\alpha x})}. \tag{1}$$

Here, I_0 is the intensity of the incident beam and I that of the transmitted beam. α is the absorption coefficient and x is the sample thickness (assumed homogeneous). R is the reflectivity from a single surface of the sample and is given by, $R = [(n-1)^2 + k^2]/[(n+1)^2 + k^2]$, where n is the refractive index and k is the extinction coefficient in the frequency region of interest.

Fourier transform infrared (FTIR) spectrometers are now widely used to measure IR absorption spectra and have much greater sensitivity and resolution than dispersive spectrometers.[15] In an FTIR instrument, a Michelson interferometer is used to measure an interferogram (intensity vs. path length difference between the arms of the interferometer) whose Fourier transform is the spectrum (intensity vs. frequency). For spectroscopic measurements, the frequency, $\overline{\nu}$, is often given in wavenumber (cm^{-1}) units, where $\overline{\nu} \equiv 1/\lambda$ is the reciprocal of the wavelength.

In Eq. (1), an interference oscillation that can occur for a sample with plane-parallel front and back surfaces has been neglected. (In practice, this interference oscillation can be reduced by wedging one of the sample's surfaces at an angle of a few degrees or by eliminating sharp peaks in an interferogram that give rise to oscillations in the spectrum.) In many cases, Eq. (1) may be simplified, and the following approximate relationship for the transmission is used:

$$T \cong (1-R)^2\, e^{-\alpha x}. \tag{2}$$

FTIR instruments can conveniently produce an absorbance spectrum from a transmission spectrum. The absorbance, A, is given by, $A = -\log_{10}(T)$.

The quantity that characterizes the absorption arising from a specific defect is its absorption coefficient, α_d. However, the α in Eqs. (1) and (2) mentioned earlier includes absorption from the host crystal, and all of the other defects it contains. To isolate α_d, it is helpful to be able to measure a reference spectrum for a sample of the host material that does not contain the defect of interest. In this case

$$\alpha_d \cong x^{-1}\, ln(T_R/T_S). \tag{3}$$

Here, T_S is the transmission spectrum for the sample containing the defect of interest, and T_R is the transmission spectrum for the reference sample. The approximate relationships [Eqs. (2) and (3)] give an absorption coefficient that is typically in error by less than 10%. If quantitative measurements with higher accuracy are required, an equation similar to Eq. (1) must be inverted to determine α (see Refs. 8 and 16, for example).

If a sample is not homogeneous, so that the thickness of the layer that contains the defect of interest is not well defined, it can be more convenient to report an absorbance spectrum, which is also given on a log scale, similar to the absorption coefficient. For a situation where both sample and reference absorbance spectra have been measured, the absorbance, A_d, associated with a defect of interest is

$$A_d = A_S - A_R = \log_{10}(T_R/T_S). \tag{4}$$

For the characterization of impurities, it is useful to be able to determine the concentration of a defect from its vibrational spectrum. The area of a vibrational absorption band (i.e., the integrated absorption coefficient) is proportional to the concentration of defects, N in units cm^{-3}, and is given by the equation[17]

$$\int \alpha(\overline{\nu})\, d\overline{\nu} = (\pi q^2 N)/(\mu n c^2). \tag{5}$$

This equation has been written in CGS units to be consistent with the absorption coefficient, α, which is conventionally determined in units cm^{-1}, and the frequency $\overline{\nu}$ given in cm^{-1}. (The integrated absorbance is proportional to the areal density of a defect in units cm^{-2}.) In Eq. (5), μ is the reduced mass of the vibrating impurity, n is the refractive index of the host crystal, c is the speed of light, and q is a parameter called the effective oscillating charge. The effective charge is not a static charge on the defect. Instead, q is the change in the dipole moment per unit displacement of the vibrational mode's normal coordinate. The effective oscillating charge is quoted typically as a multiple of the electron charge, e (in esu in CGS units).

To determine an accurate defect concentration from vibrational spectroscopy, there must be an independent calibration that relates concentration to the absorption strength because the effective charge q is unknown. Several methods have been used to determine the defect concentration, including secondary ion mass spectrometry (SIMS), activation analysis, and Hall effect. The effective charges of many defects have been determined and vary from roughly $0.3e$ to $3e$ (see Ref. 9, for example). If there is no independent determination of a defect's concentration to calibrate the IR absorption strength, a rough estimate of the concentration can be made with the approximation $q = e$. When making this approximation, it should be recognized that the error in the estimate of the concentration will typically be a factor of two to four and could be much larger.

The sensitivity limit of a LVM absorption measurement depends strongly on the defect being studied. As a rough guideline, LVMs, with a typical effective oscillating charge of $q \approx 1e$, can be detected for concentrations of the order of $10^{14}\,cm^{-3}$ in a 1-cm thick bulk sample, or $10^{18}\,cm^{-3}$ in a 1 μm-thick epitaxial layer.

2. Raman spectroscopy

It is important to note that not all vibrational modes are IR active. For example, the stretching vibration of a homonuclear diatomic molecule, at a site of high symmetry in a crystal, does not give rise to an oscillating electric dipole moment, and does not interact with the electric field of the incident light. Therefore, electric-dipole-allowed optical transitions do not occur in this case, and there is no absorption. However, Raman scattering is subject to different selection rules than the electric dipole-allowed optical transitions observed by IR-absorption spectroscopy. Therefore, Raman spectroscopy can provide information about vibrational modes

that are not IR active.[13] For example, Raman spectroscopy has been a powerful probe of interstitial H_2 molecules in semiconductors.[18]

For Raman-scattering measurements of LVMs, a monochromatic laser beam is incident on a sample. Typically, the scattered light is dispersed with a double or triple monochromator and detected with a multichannel detector. In addition to the elastically scattered light, there is also light that has been inelastically scattered by the excitations of the crystal, where here it is LVM excitations that are of interest. At low temperatures, it is primarily the scattering processes that excite impurity vibrations that have appreciable intensity. In this case, the frequency $\overline{\nu_S}$ of the scattered light that excites a LVM, satisfies the relationship

$$\overline{\nu_S} = \overline{\nu_L} - \overline{\nu_{LVM}}, \tag{6}$$

where $\overline{\nu_L}$ and $\overline{\nu_{LVM}}$ are the laser and LVM frequencies, respectively. Therefore, LVM frequencies can be determined from their Raman shifts.

Raman scattering is also advantageous for measurements of thin, heavily doped, semiconductor layers, where it is difficult to measure IR-absorption spectra because of the strong competing absorption that results from free carriers.[13] Another advantage of Raman scattering is that both polarized and depolarized scattering can be measured to provide information about the symmetry of an LVM.

A disadvantage of Raman scattering is that the Raman effect is a weak process. To obtain sufficient Raman-scattered intensity to study defects, the energy of the incident light often must be selected to match the energy of transitions to high-lying, electronic energy bands of the host crystal so that the scattered intensity might be resonantly enhanced by a few orders of magnitude.[19] With GaAs, for example, incident photon energies near 2–3 eV are typically used. Another disadvantage of Raman scattering is that the resolution, which typically has been achieved in experiments, is a few cm^{-1} and is not sufficient to resolve the small frequency shifts that result from the different isotopes of an impurity's nearest neighbors that will be discussed in Sec. II B.

B. Role of isotopes

For an LVM that is localized at an impurity atom and its nearest neighbors, a model of a simple diatomic "defect molecule" provides much physical intuition about the impurity's vibrational properties.[9,20] When a light-mass impurity is attached to a heavier host atom (Fig. 1), the vibrating mass is the reduced mass of the impurity and its neighbor. The vibrational frequency, $\overline{\nu}$, of the diatomic molecule is given by Eq. (7), where k is a force constant, m_i is the mass of the impurity, and M_n is the mass of the host atom to which the impurity is attached

$$\overline{\nu}^2 = k\left(\frac{1}{m_i} + \frac{1}{XM_n}\right). \tag{7}$$

The mass of the host atom has been multiplied by the factor X to account for its being bonded to the rest of the crystal. X may be greater than or less than 1 for light-mass elements in semiconductors.[20] Equation (7) shows that the vibrational frequency provides information about the mass of the light-element impurity and the mass of the host atom to which it is attached. Furthermore, the effect of isotopic substitutions for the impurity or host atoms often makes an unambiguous identification possible for the defect atom(s) and its neighbors.

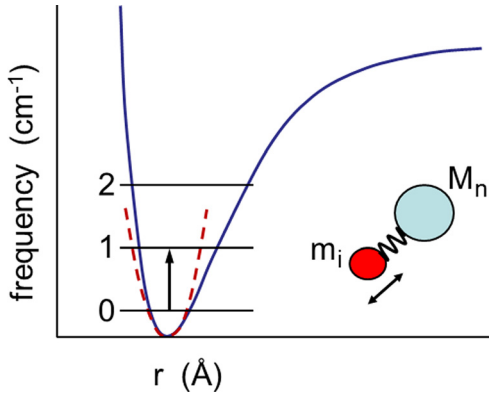

FIG. 1. Schematic of the anharmonic potential of a diatomic molecule used as a model for a light-mass impurity with mass m_i bonded to a host atom with mass M_n.

The high spectral resolution that is possible with commercial FTIR instruments allows the small frequency shifts of impurity modes that result from a change in the isotopic mass of the nearest neighbors of a light impurity to be observable. (A spectral resolution of 0.1 cm^{-1} is adequate for most LVM studies in semiconductors.) A few impurities can be conveniently characterized at room temperature. Most studies, however, are performed with samples held at temperatures near 77 K or 4.2 K. At low temperature, a LVM line narrows and its peak absorption coefficient increases. Thus, the sensitivity of the IR measurement is increased, and small frequency shifts can be resolved.

A defect may contain more than one light-mass element. In this case, a coupling of the vibrational modes can lead to shifts and splitting of the vibrational lines. For example, for a defect that contains two identical H atoms, these vibrational modes will become coupled to form antisymmetric and symmetric modes with a frequency difference between them.

Isotopic substitutions help to reveal the coupling of identical modes (or modes that lie close in frequency). For example, if both H and D are introduced into a host crystal that contains a defect with two H atoms, there will also be defects formed with both H and D. The H and D modes of the defect will be dynamically decoupled because of the large difference in the masses of H and D. The additional vibrational lines that result from the defects that contain both H and D prove that the defect of interest contains two H atoms, and reveals the coupling of the modes and their coupling strength.

The different impurity isotopes and the natural abundances of the host-atom isotopes help to identify the atoms in a defect complex with vibrational spectroscopy. Remarkably, it is now possible to also engineer the isotopic content of the host crystal, further expanding the capabilities of vibrational spectroscopy as a strategy for determining the microscopic properties of defects containing the light-mass elements.[21]

The following two sections, Secs. II B 1 and II B 2, describe classic examples of impurities whose identities and microscopic structures have been determined from the isotope dependence of their vibrational spectra.

1. Oxygen in Si

Oxygen in an important impurity in Si (Ref. 22) and is an early example of a defect in a solid whose configuration and microscopic properties were determined by vibrational spectroscopy.[23,24] The absorption spectrum of the antisymmetric-stretching mode of interstitial oxygen in Si is shown in Fig. 2. Oxygen sits at an interstitial position and interrupts the bond between two Si nearest neighbors, as is shown in the inset.[25,26] The strong line at 1136.4 cm^{-1} is due to the antisymmetric-stretching mode of the ^{28}Si-^{16}O-^{28}Si "defect molecule."

The spectrum shown in Fig. 2 was measured for a sample that had been enriched with ^{17}O and ^{18}O. The antisymmetric-stretching line is shifted to lower frequencies for the heavier oxygen isotopes, proving that the 1136.4 cm^{-1} line is due to an ^{16}O vibrational mode. The vibrational structure observed for each oxygen isotope, with a strong line and two weaker satellite lines at lower frequencies, is due to the naturally abundant isotopes of Si, ^{28}Si (92.23%), ^{29}Si (4.67%), and ^{30}Si (3.10%). (The strongest line is due to the ^{28}Si-^{16}O-^{28}Si configuration and the two weaker satellites are due to ^{29}Si-^{16}O-^{28}Si and ^{30}Si-^{16}O-^{28}Si.) The relative intensities of the lines that arise from the different Si isotopes show that two Si atoms are involved in the LVM. A model for the frequencies of the isotopic structure shown in Fig. 2 yielded a Si-O-Si bond angle of 164 °.[25,26]

In addition to the antisymmetric stretching mode of interstitial oxygen, there are also a forbidden symmetric-stretching mode,[26] a low frequency quasi-localized mode with a fascinating tunneling character,[27] and a combination mode near the sum frequency of the antisymmetric and symmetric stretching modes.[26,28]

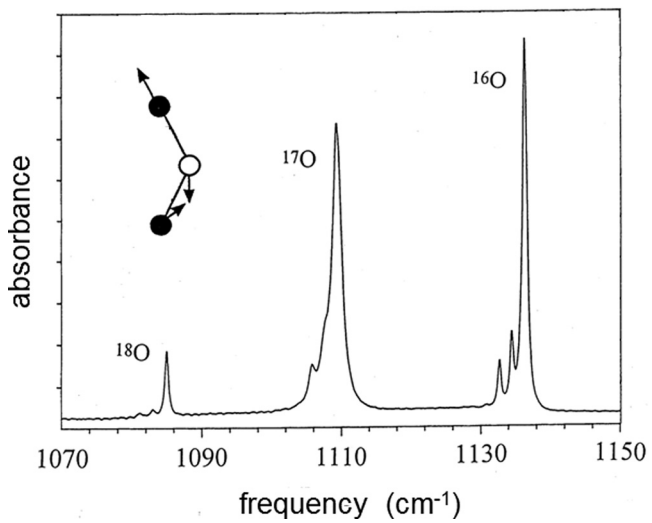

FIG. 2. Spectrum measured at liquid He temperature for a Si sample enriched with ^{17}O and ^{18}O showing the antisymmetric stretching mode of interstitial oxygen. The inset shows the configuration of the oxygen and Si atoms and their motion for the antisymmetric stretching mode. [Adapted with permission from Pajot *et al.*, J. Phys.: Condens. Matter **7**, 7077 (1995) Copyright 1995 IOP Publishing Ltd.]

2. Silicon in GaAs

The vibrational spectrum of the Si impurity in GaAs provides another example of how vibrational spectroscopy can reveal the detailed local structure of a defect.[29,30] At concentrations of less than 10^{18} cm^{-3} in stoichiometric GaAs, a Si impurity occupies a Ga site (Si_{Ga}), where it acts as a donor. At higher concentrations or in Ga-rich material, Si can occupy an As site (Si_{As}), where it acts as an acceptor.

The site where the Si impurity sits can be identified by vibrational spectroscopy.[31] Si_{Ga} has a vibrational line at 384 cm^{-1} (Fig. 3). This line is relatively sharp because the Si_{Ga} defect has four identical ^{75}As first neighbors because the ^{75}As isotope is 100% abundant. There is an additional band due to the Si impurity at 399 cm^{-1}. However, Fig. 3 shows that this band has several near-lying components. The 399 cm^{-1} band has been assigned to Si_{As} whose spectral structure arises from the different possible concentrations of ^{69}Ga (60%) and ^{71}Ga (40%) isotopes in the Si_{As} defect's first neighbor shell.[9,29,31]

(A substitutional carbon impurity in GaAs has a multi-component vibrational band at 582 cm^{-1} that is similar in structure to the Si_{As} band at 399 cm^{-1}. C occupies only an As sublattice site in GaAs with ^{69}Ga and ^{71}Ga first neighbors, where it acts as an acceptor.[9,31,32])

C. Theory

Density functional theory based on supercells is the standard starting point for the theoretical treatment of defect structures and properties in systems of interest.[33] A "superlattice" is constructed of large identical unit cells, each of which contains the defect, and the many-electron problem is solved using large, complex computer codes.[33–37] Stable and metastable defect structures, electrical level positions, vibrational frequencies, and other physical properties may be obtained from

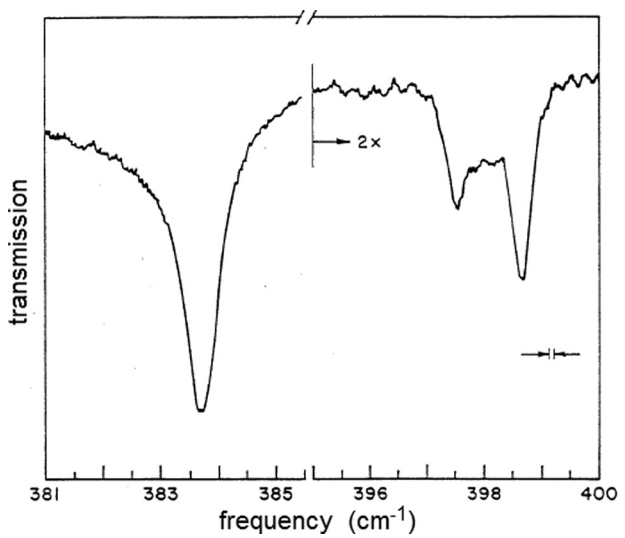

FIG. 3. The absorption bands assigned to the LVMs of Si_{Ga} (left) and Si_{As} (right) in GaAs. [Reproduced with permission from Theis *et al.*, Appl. Phys. Lett. **41**, 70 (1982). Copyright 1982 American Institute of Physics.]

these methods. While the most common approaches involve expanding the electronic wave functions in plane waves,[34] alternative expansions based on local atomic-like orbitals have also proved tractable.[35–37]

The combination of theory and experiment can yield powerful, unambiguous information about the nature and structure of particular defects. Thus, for example, polarized-light experiments can yield the direction of the O-H dipole in a defect; calculations on various candidate defect structures can eliminate many, and may yield only one that satisfies the O-H dipole direction.

Furthermore, for defects involving two hydrogens (two O-H dipoles), measurements for H-doped, D-doped, and H and D co-doped can reveal whether the two O-H sites are equivalent by symmetry and how strongly coupled they are, along with significant polarization information, all of which can also be calculated by theory.

D. Anharmonicity

The potential energy function shown for the defect molecule in Fig. 1 is anharmonic. The anharmonicity of a vibrational mode plays an important role in solids just as it does in molecules. The fundamental mode of vibration (the transition with $n = 0$ to $n = 1$ in Fig. 1) typically dominates the vibrational spectrum. Weak overtones (for example, the transition with $n = 0$ to $n = 2$ in Fig. 1) and combination modes, allowed by anharmonicity of the vibration, are also sometimes observed.

In Eq. (7), the assumption has been made that the vibration of the impurity is perfectly harmonic. In practice, the large amplitude of the vibrational motion, especially for very light atoms, with hydrogen being a good example, causes anharmonicity to have a significant effect on an impurity's vibrational frequencies.[20]

Anharmonicity causes the observed vibrational frequency to be less than the harmonic frequency, a fact that is important for the comparison of experimental vibrational frequencies with the results of theory.[20,38,39] The following expression resulting from a Morse potential is often used to account for the anharmonic term values:

$$G(n) = \hbar\omega_e\left(n+\frac{1}{2}\right)\left[1 - x_e\left(n+\frac{1}{2}\right)\right]. \tag{8}$$

Here, ω_e and x_e are each proportional to $\mu^{-\frac{1}{2}}$, where μ is the reduced mass of the vibrating impurity. The transition energy is then

$$\Delta G_{n0} = n\hbar\omega_e\,[1 - x_e(n+1)]. \tag{9}$$

Anharmonicity affects not only the energies but also the transition probabilities between levels.[20,38,40] For a harmonic system, the only transition from the ground state, $n = 0$, will be to the first excited state, $n = 1$. In the anharmonic case overtones, usually weak, may be observed to higher-n states. As noted in Sec. II A 1, the transition matrix element involves the change in the dipole moment as a function of M_n-m_i separation, where M_n is the heavy atom to which the light atom m_i is attached. This may be nonlinear, resulting in enhanced or diminished transition rates to higher states.

The anharmonic interaction between vibrational modes affects the vibrational lifetimes of localized impurity modes through the coupling of the impurity vibrations to lower frequency modes of the solid which can be localized or delocalized.

III. ADDITIONAL PERTURBATIONS

Additional perturbations extend the capabilities of vibrational spectroscopy and provide further information about the microscopic properties of a defect. Here, the effects of charge state changes, uniaxial stress, and hydrostatic pressure are discussed.

A. Change of charge state and effect of illumination

Many defects are electrically active and have levels in the semiconductor band gap. A change in the charge state of a defect changes the amount of charge localized in the bonds and, therefore, shifts the vibrational frequencies. For a shallow impurity, a change of charge state has little effect on the vibrational frequency because the wave function of a bound carrier is delocalized, and the force constants of the bonds near the defect are not strongly affected. However, a deep-level defect has more localized electronic wave functions, and the shift in the vibrational frequency upon a change of charge state is typically tens of cm^{-1}.

The same defect can have different vibrational frequencies in samples with different positions of the Fermi level, for example, in n-type vs p-type material, because its charge state might be changed.[6,41] An alternative method to modify the charge state of a defect is by photoionization with an additional source of illumination. When the defect is photoionized, the intensity of a vibrational line associated with the equilibrium charge state is reduced, and the intensity of a line associated with a photo-populated charge state is increased. Such measurements have been used to show that a defect is electrically active and to identify the vibrational lines of the different charge states. The spectrometer's illumination source can also photoionize the defects in a sample and, therefore, the charge states seen in an experiment are not necessarily the equilibrium charge states. The spectrometer light can be filtered to reduce the effect of photoionization.

B. Uniaxial stress

Uniaxial stress is often used in conjunction with vibrational spectroscopy to provide additional information about a defect's symmetry and the kinetics of its motion.[10,42] A defect in a crystal lattice can have several crystallographically equivalent orientations, consistent with its symmetry.[43] For example, a defect with trigonal symmetry in a diamond or zinc blende lattice can have its threefold axis oriented along any of the $\langle 111\rangle$ crystal axes. An applied uniaxial stress can make the different orientations of a defect inequivalent, and give rise to orientation-dependent shifts of the defect's vibrational frequencies and ground state energy. The shifts of the vibrational frequencies can cause the LVM lines

to be split into components. The shift of the ground state energy can cause particular orientations of the defect to be preferentially populated.

In stress experiments, stresses are applied to oriented samples along a few high symmetry crystal directions, typically [001], [111], and [110]. Absorption measurements are made with light beams that are polarized parallel and perpendicular to the stress direction. In most cases, the defect cannot reorient if the temperature is sufficiently low, and the vibrational lines are simply split into components by the applied stress. The number and relative intensities of the stress-split components depend on the orientation of the stress, the polarization of the probing light, and the symmetry of the defect. A comparison of the data measured for a few orientations of the stress with stress-splitting patterns that have been tabulated in the literature[43] for the different possible point groups is often sufficient to determine a defect's symmetry.

At elevated temperatures, some defects have sufficient thermal energy to reorient in the lattice.[10] In this case, when a stress is applied, which makes the ground state energies of differently oriented defects inequivalent, the different orientations will be populated according to Boltzmann statistics if sufficient time elapses for equilibrium to be established. If the sample temperature is reduced with the stress applied, the alignment of the defect can be frozen in and will remain, even after the stress is removed. The stress-induced alignment can be detected by the dichroism in the LVM absorption lines, i.e., from the difference in absorption strength for light beams polarized parallel and perpendicular to the stress direction. When the sample is annealed in the absence of stress, the different orientations will become randomly populated, and the stress-induced dichroism will disappear. The annealing kinetics of the dichroism can be studied to determine the height of the energy barrier for reorientation. In some cases, the atomic motion by which a defect reorients is also a diffusion jump, and the diffusion constant for the defect can be determined from the measurements of the kinetics of single diffusion jumps by vibrational spectroscopy.

C. Hydrostatic pressure

Hydrostatic pressure provides an additional method to perturb and study defect properties.[11] In elegant experiments, a sensitive infrared detector was integrated with a diamond anvil cell to make it possible to measure the IR absorption spectra of LVMs over a wide range of hydrostatic pressures.[44] Under pressure, the configuration of a defect is perturbed. The defect force constants and bond angles can be modified to shift vibrational frequencies or tune the interactions between the near-lying modes. For example, the Si-O-Si bond angle α, shown in the inset in Fig. 2 for oxygen in Si, is decreased by hydrostatic pressure, changing the character of a low-frequency mode of the defect seen in the far-infrared from that of a perturbed harmonic oscillator[27] to that of a rotator.[45] Furthermore, pressure can induce more drastic changes in the configuration of a defect, which can be investigated by the changes in the defect's vibrational properties.[44]

IV. NOVEL PROPERTIES OF DEFECTS FROM THEIR VIBRATIONAL SPECTRA

The following sections, Secs. IV A–V D, survey a growing number of situations where vibrational spectroscopy reveals novel properties of defects, taking us beyond the identification of the defect atoms and their microscopic structure.

A. Vibrational lifetimes

The local vibrational modes of impurities in semiconductors have been studied for 60 years. However, only recently have the vibrational line widths and their relationship to the lifetimes of the excited vibrational modes begun to be studied and understood by experiment and theory.[12,46,47]

Hydrogen defects in Si have provided fascinating model systems for studies of vibrational lifetimes and line widths. In addition to isolated bond-centered hydrogen,[48] these defects include the Si vacancy with its Si dangling bonds decorated by different numbers of H atoms (VH_n),[49] a Si interstitial with its two dangling bonds decorated by H (IH_2),[50] a hydrogenated Si divacancy (V_2H_2),[51,52] and a hydrogen dimer called H_2*.[53] The lifetimes of the Si-H stretching and bending modes for several of these defects have been measured directly by transient bleaching methods. These measured lifetimes have been found to be in excellent agreement with the vibrational line widths (measured at 4.2 K for hydrogenated samples with defects produced by electron irradiation) as determined by the uncertainty principle, $\Gamma_1 = 1/(2\pi c\tau)$, where Γ_1 is the line width (in cm^{-1}) and τ is the vibrational lifetime.[48,52,54]

The H_2* defect is shown in the inset to Fig. 4(a) and contains one H atom at a bond-centered site (H_{BC}) and a second H atom at an antibonding site (H_{AB}) along the same three-fold axis.[53] Transient bleaching data[55] shown in Fig. 4(a) acquired for the H_{AB} bending mode of the H_2* defect determine that this mode's vibrational lifetime is 12.2 ps. Figures 4(b) and 4(c) show the spectra of the H_{AB} and D_{AB} bending modes of the H_2* and D_2* defects, respectively. The line width for H_{AB} yields a vibrational lifetime of 12.6 ps, in excellent agreement with the transient bleaching result. The line width for D_{AB} yields a vibrational lifetime of 10.4 ps.

The lifetimes of the hydrogen bending modes of a variety of defect complexes have been found to obey a frequency gap law (Fig. 5), where the lifetime depends exponentially on the number of phonons involved in the relaxation process.[55] However, the measured vibrational lifetimes (and line widths) of the Si-H stretching modes of the hydrogenated lattice defects do not show such regular behavior, and have been found to vary by more than a factor of 100, with the V_2H_2 defect having a lifetime of 291 ps, and the H_2* defect having a lifetime of 4.2 ps.[54] Theory has suggested mechanisms to explain the widely varying lifetimes of the Si-H stretching modes of the hydrogenated lattice defects.[47] For example, the short vibrational lifetime of the Si-H modes of H_2* is predicted to be caused by the interaction of the two nearby hydrogen stretching modes of the defect, and their exchange of vibrational energy.

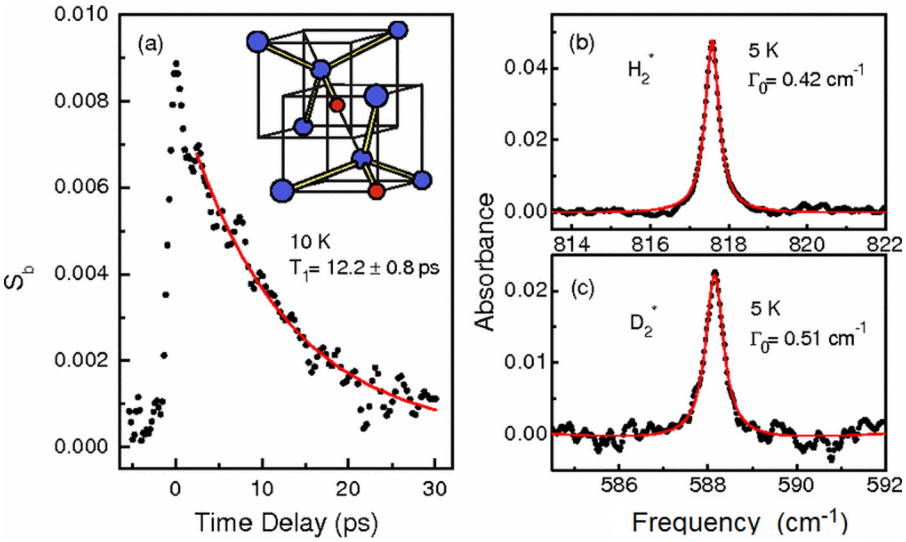

FIG. 4. (a) The transient bleaching signal of the bending mode of H_2* in Si. The structure of the H_2* defect is shown in the inset. (b) and (c) show the absorption spectra of the H- and D-bending modes of H_2* and D_2*, respectively. [Reproduced with permission from Sun *et al.*, Phys. Rev. Lett. **96**, 035501 (2006). Copyright 2006 American Physical Society.]

The lifetimes of the vibrational modes of the light elements can depend strongly on the accidental coincidence of the vibrational mode frequencies. In this case, isotopic substitutions that make small changes in the mode frequencies can have dramatic effects on the vibrational lifetimes.[56,57]

B. Oxygen diffusion in Si

Interstitial oxygen in Si interrupts a Si-Si bond along a ⟨111⟩ direction in the diamond cubic lattice.[25,26] When stress is applied along either a ⟨110⟩ or ⟨111⟩ direction, the different orientations for oxygen become inequivalent. Corbett *et al.* found that if stress is applied at temperatures near 400 °C, the interstitial oxygen center can be preferentially aligned by the applied stress.[58] If the sample is then cooled with the stress maintained, the alignment of the oxygen center becomes frozen in. This alignment resulted in a dichroism for the oxygen vibrational band at 1106 cm^{-1} (room temperature), that is, a difference in absorption for light beams polarized perpendicular and parallel to the stress direction.

Figure 6 shows the spectra for an interstitial oxygen impurity in Si that has been aligned by stress with the electric vector of the probing light oriented perpendicular and parallel to the stress direction. The increased absorption of oxygen in the anti-symmetric vibrational mode shows that orientations with no component along the stress direction have lower ground state energies and become preferentially populated.

For a Si sample for which preferentially aligned oxygen centers have been quenched in (by cooling from 400 °C to room temperature under stress), subsequent annealing experiments in the absence of stress will cause the different orientations to become randomly populated. The time constant for a jump of oxygen from one site to another (inset to

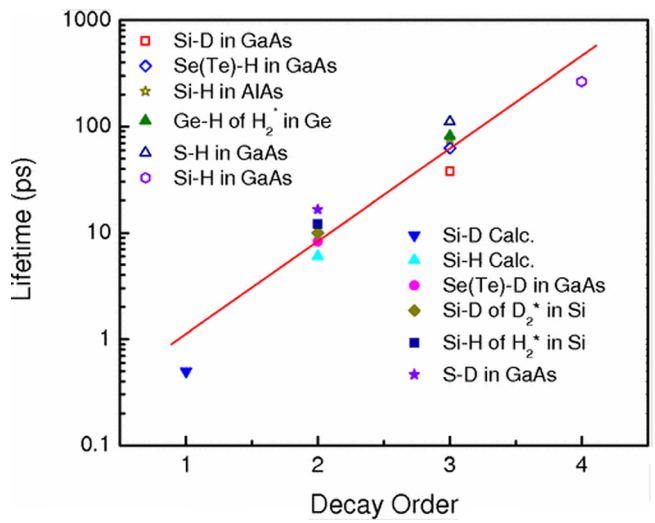

FIG. 5. Vibrational lifetimes of H-related bending modes vs their decay order in different hosts. The line shows that the lifetimes obey a frequency-gap law where the lifetime depends exponentially on the decay order. [Reproduced with permission from Sun *et al.*, Phys. Rev. Lett. **96**, 035501 (2006). Copyright 2006 American Physical Society.]

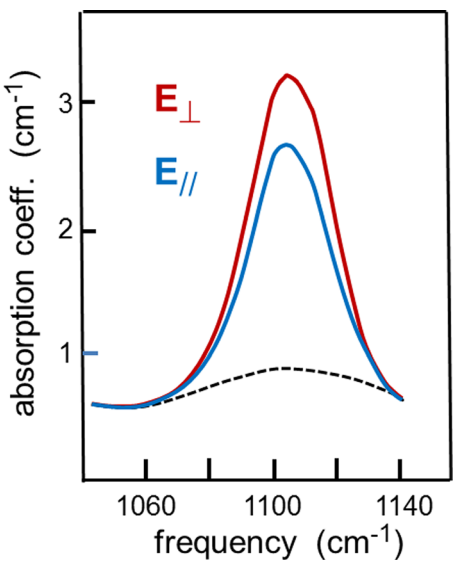

FIG. 6. The 1106 cm^{-1} absorption band for interstitial oxygen in Si (room temperature) following the application of a ⟨111⟩ stress at 400 °C for 30 min. Spectra for $E_\perp$ (red) and $E_{//}$ (blue) are for polarizations of the probing light perpendicular and parallel to the stress axis, respectively. (The dashed line shows the absorption from the Si lattice.) [Adapted with permission from Corbett *et al.*, J. Phys. Chem. Solids **25**, 873 (1964).]

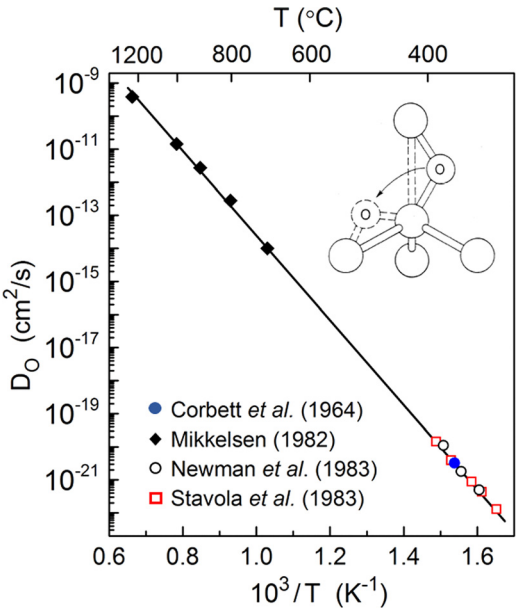

FIG. 7. Diffusion constant vs 1/T for interstitial oxygen in Si. The inset shows the configuration of interstitial oxygen in Si and a diffusion jump from one interstitial site to another. (From the oxygen diffusivities reported in Refs. 58–61.)

Fig. 7) can be determined from the kinetics of the decay of the dichroism.[58]

For oxygen in Si, the process by which the dichroism is annealed away is also a diffusion jump. In this case, the diffusion constant, D_O, of oxygen is given by the relationship

$$D_O = d^2/(8\tau) = a^2/(12\tau),$$

where d is the jump distance from one bond-centered site for oxygen to another, a is the Si-Si nearest neighbor distance, and τ is the time constant for the decay of the dichroism.[58–60]

Interstitial oxygen in Si plays an important role in the processing of Si integrated circuit materials,[22] and its diffusion constant has been of substantial interest. The diffusion constant for oxygen has been measured for temperatures above ~600 °C primarily with mass transport measurements[61] and at temperatures below ~400 °C with stress alignment methods.[58–60] The diffusion constant for oxygen in Si is shown in Fig. 7 for over 12 decades in the diffusivity![10,61–63]

C. DX configuration of Si_{Ga} in GaAs under pressure

The substitutional Si_{Ga} shallow donor in GaAs discussed in Sec. II B 2 can undergo a configurational transition from an ordinary shallow donor to an unusual deep-level defect known as the DX center, which was found to exhibit persistent photoconductivity.[64–66] The transformation of the Si impurity from a shallow defect to the DX configuration occurs in GaAs under hydrostatic pressures greater than ~20 kbar, in $Al_xGa_{1-x}As$ alloys with Al content $x \geq 0.22$, and at Si doping concentrations that exceed 10^{19} cm^{-3}. (Other donor impurities and additional compound semiconductors also exhibit transitions to deep DX states.) The DX center and its unusual behavior have been studied extensively.[64–66]

A theoretical model proposed by Chadi and Chang for this configurational transformation predicts that the

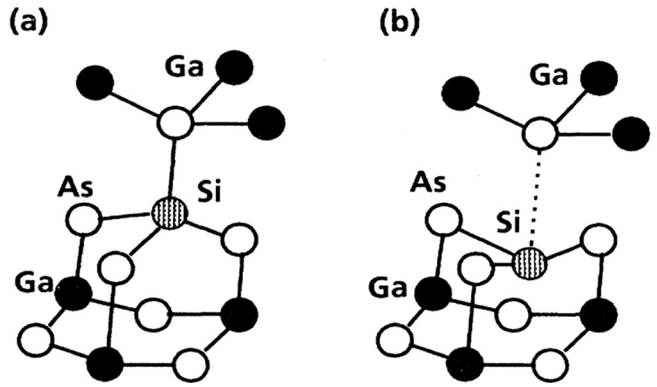

FIG. 8. (a) Substitutional site of Si_{Ga} in GaAs. (b) The broken-bond DX configuration for Si in GaAs. [Adapted with permission from Chadi and Chang, Phys. Rev. B **39**, 10063 (1989). Copyright 1989 American Physical Society.].

substitutional Si_{Ga} atom undergoes a large lattice relaxation in which the Si atom is displaced along a ⟨111⟩ direction.[67,68] Figure 8(a) shows a Si atom at a Si_{Ga} site where it is bonded to four As atoms and acts as a shallow donor. Figure 8(b) shows the predicted DX configuration where one Si-As bond has been broken, and the Si atom has been displaced along a ⟨111⟩ direction to be bonded to three As atoms.

In technically beautiful experiments performed by Wolk *et al.*, an IR detector was integrated with a diamond anvil cell to make it possible for the IR absorption spectra of LVM's to be measured as a function of applied hydrostatic pressure.[44] Figure 9 shows the frequencies of the vibrational lines that were seen for GaAs:Si samples as a function of the applied pressure. At pressures less than ~20 kbar, a single vibrational line was seen with a zero-pressure frequency of 384 cm^{-1}, which is due to the Si_{Ga} shallow donor. At pressures exceeding 20 kbar, an additional vibrational line emerged with a frequency that is 10 cm^{-1} less than that of the Si_{Ga} line. It was also found that the sample showing the new pressure-induced vibrational line exhibited persistent photoconductivity. The new pressure-induced line was assigned to the DX center associated with Si in GaAs.

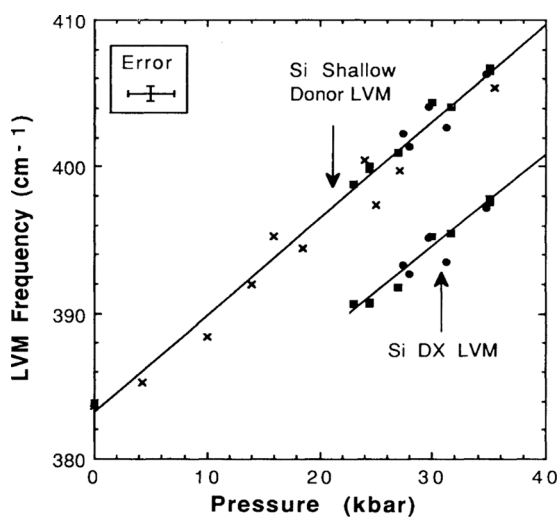

FIG. 9. Dependence of the Si_{Ga} and Si DX vibrational frequencies for GaAs under hydrostatic pressure. [Reproduced with permission from Wolk *et al.*, Phys. Rev. Lett. **66**, 774 (1991). Copyright 1991 American Physical Society.]

In these experiments, the vibrational modes of both the Si_{Ga} shallow donor and the DX center were seen along with the pressure-induced configurational transition between them.[44] The vibrational properties of the DX center have also been investigated by theory.[69]

D. Oxygen in GaAs and the negative U of the V_{As}-O center

The oxygen impurity in GaAs has been found to have two possible structures that were identified by the isotopic structure of their vibrational lines.[70] Furthermore, one of these defects has been discovered to be a center with multiple charge states and a negative U.[71,72]

The vibrational bands at 845 and 715 cm^{-1} shown in Figs. 10(a) and 10(b) were shifted to 802 and 679 cm^{-1}, respectively, when ^{18}O was substituted for ^{16}O. These oxygen related shifts show that these bands can be unambiguously assigned to vibrational modes of oxygen. The bands at 845 and 715 cm^{-1} also show isotopic structures that have been attributed to the Ga and As isotopes of the oxygen atom's first neighbors.

Figure 10(a) shows that the 845 cm^{-1} band is split into two components. This vibrational spectrum is consistent with the defect structure shown in the inset to Fig. 10(a) where an interstitial oxygen atom interrupts an As-Ga bond. The natural isotopic abundances of the As and Ga isotopes are As (100%), ^{69}Ga (60%), and ^{71}Ga (40%), giving rise to two possible isotopic configurations for the interstitial oxygen defect and its As and Ga first neighbors. (This structure is similar to that of the interstitial oxygen defect in Si.[25,26])

Figure 10(b) shows that the 715 cm^{-1} line is split into three near-lying components. This structure is consistent with an off-center oxygen atom at an As vacancy, V_{As}-O, which is bonded to two Ga neighbors as is shown in the inset to Fig. 10(b). The ^{69}Ga and ^{71}Ga isotopes give rise to three different first-neighbor configurations (^{69}Ga-O-^{69}Ga, ^{71}Ga-O-^{71}Ga, ^{69}Ga-O-^{71}Ga), consistent with the three components of the 715 cm^{-1} band and their relative intensities. (This structure is similar to that of the well-known A-center in Si, which consists of an off-center oxygen atom at a Si vacancy.[73])

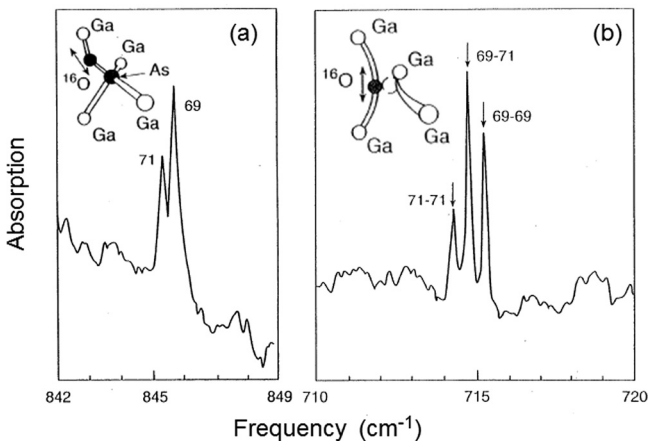

FIG. 10. Absorption spectra (4.2 K) for (a) interstitial oxygen in GaAs and (b) the off-center O-V_{As} complex in GaAs. The structures of the defects are shown in the insets. [Adapted with permission from Schneider *et al.*, Appl. Phys. Lett. **54**, 1442 (1989). Copyright 1989 American Institute of Physics.]

The V_{As}-O center that gives rise to the 715 cm^{-1} band has additional charge states.[71,72,74] Figure 11 shows that there are, in fact, three different vibrational bands in GaAs at 730.6, 714.2, and 714.9 cm^{-1} with the same triplet isotopic structure. Studies of the optical and thermal conversions of the V_{As}-O center between its different charge states led to the conclusion that these bands correspond to charge states with zero (band A), one (band B'), and two (band B) bound electrons, and that V_{As}-O is a negative U defect.[71,72] (For a negative U defect, the unusual situation occurs where the second bound electron has greater binding energy than the first making the charge state with one bound electron metastable.) Theory has also been used to investigate the multiple charge states of the V_{As}-O defect.[74]

The illumination-induced conversion between charge states of the V_{As}-O defect and the discovery of its negative U properties were revealed by investigations of its vibrational spectrum.

E. The nuclear-spin states of interstitial H_2 in semiconductors

H_2 in gas phase is a fascinating molecule for which the influence of nuclear spin on the molecular wave function was revealed in the 1920s.[75] The H_2 molecule has ortho and para states with the nuclear spins of the two protons aligned either parallel (ortho) or antiparallel (para). Because the total molecular wave function of H_2 must be antisymmetric upon exchange of the two identical protons, ortho H_2 has rotational states with odd values of the rotational quantum number J, whereas para H_2 has rotational states with even J. The lowest energy state of para-H_2 has rotational quantum number $J = 0$; the lowest energy state of ortho-H_2 has rotational quantum number $J = 1$. In many circumstances, these behave

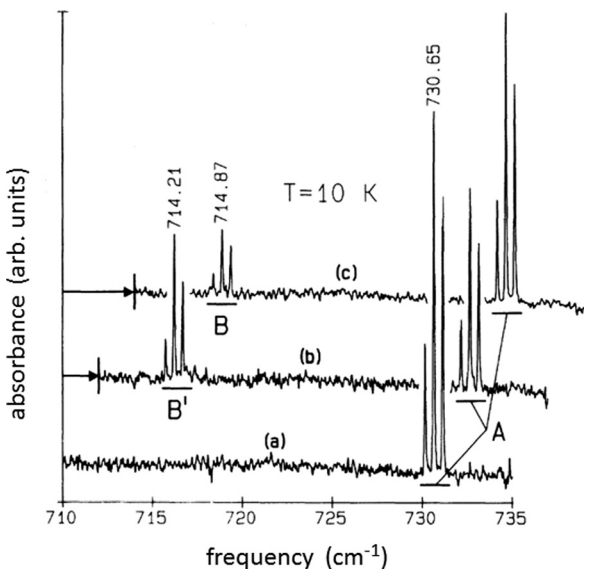

FIG. 11. Absorption spectra of semi-insulating GaAs for the Ga-O-Ga defect in its different charge states: (a) after cooling in the dark, (b) after illumination with 1.37 eV light, and (c) after warming to 95 K and cooling to 10 K. [Adapted with permission from H. C. Alt, Phys. Rev. Lett. **65**, 3421 (1990). Copyright 1990 American Physical Society.]

as two distinct molecular species, each with its own rotational spectrum.

The interstitial H_2 molecule was suggested by theory to be an important defect in semiconductors in the early 1980s.[76,77] It was not until a dozen years later that the H_2 stretching line for molecular H_2 in GaAs was discovered at 3934 cm^{-1} by Raman spectroscopy and was found to be split into two components 8 cm^{-1} apart.[78] These components were assigned to ortho and para H_2. This interpretation led to the conclusion that H_2 in GaAs is rotating freely, and that vibrational spectroscopy can provide information about the nuclear-spin state of the defect. Figure 12 shows the vibrational lines for H_2, HD, and D_2 in GaAs. The H_2 line in Fig. 12 is, in fact, two closely spaced lines due to the ortho and para nuclear spin states of the molecule. (The D_2 line also consists of two components, but these are not resolved in Fig. 12.)

As a defect in Si, the vibrational spectroscopy of the interstitial H_2 molecule was not so readily interpreted.[79] Raman and IR lines were discovered for H_2 in Si at 3618 cm^{-1} (4 K).[80,81] (Surprisingly, an IR line is weakly allowed for H_2 in Si.) However, in these early measurements, no ortho-para splitting, similar to that seen in GaAs, was observed.

Subsequent IR absorption studies of the vibrational transitions of HD in Si clarified this situation. The proton and deuteron are not identical nuclei, so the HD molecule does not have ortho and para states. The transitions between all of the rotational states of HD are possible. Rotational structure was observed for the vibrational line of HD in Si, establishing that HD (and therefore, also H_2 and D_2) is freely rotating.[82–84] With this insight, subsequent studies of H_2 in Si by Raman spectroscopy revealed the ortho-para splitting of the H_2 vibrational line (Fig. 13).[85,86] (IR spectroscopy shows only an absorption line for ortho-H_2 because of optical selection rules, so an ortho-para splitting is not seen directly.[82,83])

At elevated temperature (room temperature is sufficient), the ratio of ortho to para H_2 in Si is 3:1, consistent with the degeneracies of the ortho and para nuclear spin states. If one waits for a sufficiently long time at low temperature, the interstitial H_2 molecule can relax to its lower energy para state. This transition rate is slow because the nuclear spin of the proton interacts only weakly with its environment. With the ortho and para states of H_2 clearly visible in Raman experiments, the ortho-para transition of H_2 in Si could be studied.[86]

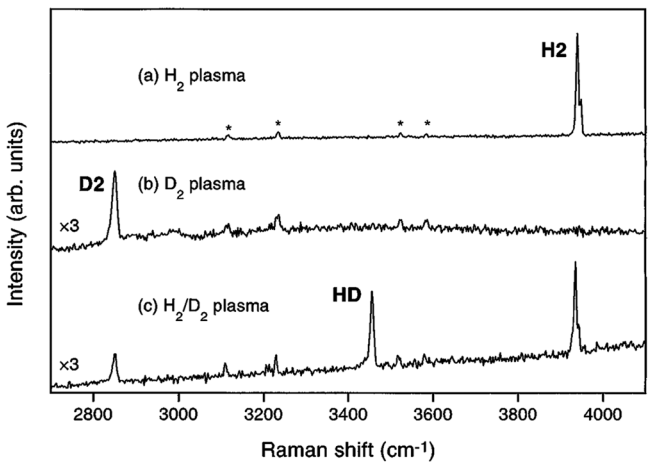

FIG. 12. Raman spectra of GaAs after treatments in (a) H_2-, (b) D_2-, and (c) H_2/D_2-containing plasmas. Note the ortho-para splitting of the H_2 stretching line. [Reproduced with permission from Vetterhöffer *et al.*, Phys. Rev. Lett. **77**, 5409 (1996). Copyright 1996 American Physical Society.]

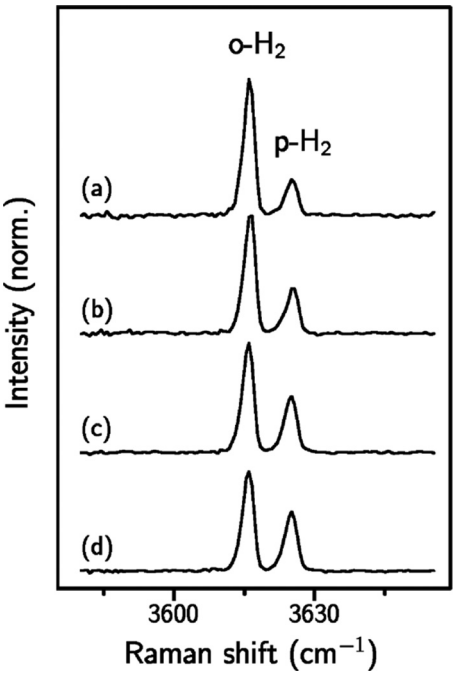

FIG. 13. Raman spectra of the H_2-stretching mode of interstitial H_2 in Si after the sample was held at 77 K for (a) 0 h, (b) 87 h, (c) 338 h, and (d) 999 h. [Reproduced with permission from Hiller *et al.*, Phys. Rev. Lett. **98**, 055504 (2007). Copyright 2007 American Physical Society.]

Figure 13 shows the Raman lines of ortho and para H_2 in Si for a sample held for an extended time at 77 K. The intensity of the para species increases as ortho-H_2 is slowly converted to the lower energy para state at 77 K.[86] [Spectrum (d) in Fig. 13 shows the result following a 999 h treatment at 77 K.] The ortho-para transition of H_2 in Si could also be studied by IR spectroscopy, where it was observed that the vibrational line due to ortho-H_2 weakened as ortho-H_2 molecules were converted into the para state that cannot be observed by IR absorption spectroscopy.[87] The time constant for the conversion of ortho-H_2 to para-H_2 was determined to be 229 h at 77 K in an IR absorption study of the ortho to para transition.[87]

Ortho-para splittings and transitions have been seen in a few additional situations. Interstitial H_2 in Si can become weakly bound to an interstitial oxygen impurity.[88] In this case, the H_2 vibrational lines reveal the ortho and para states of the O-H_2 defect.[89,90] Furthermore, the oxygen vibrational line of the O-H_2 complex becomes split into two components because the oxygen vibrational frequency depends on whether the oxygen impurity is bound to ortho or para H_2.[89]

Ortho-para splitting has also been observed for interstitial H_2 in Ge (Ref. 91) and in ZnO (Ref. 92) by Raman spectroscopy. For H_2 in ZnO, the ortho-para transition has also been investigated.[93]

V. SEMICONDUCTING OXIDES

The semiconducting oxides have attracted much recent attention as transparent conductors and wide band gap semiconductors.[94,95] Theory has played a leading role in predicting the properties of hydrogen-containing defects.[96] In several situations, experiment has confirmed the structures of defects and revealed their unusual properties via their predicted vibrational properties.[97]

A. Hydrogen as a source of n-type conductivity in transparent conducting oxides

The passivation of dopants and defects in semiconductors by hydrogen is well-known and has an impact on semiconductor technology that is widely recognized.[98] Vibrational spectroscopy has been a rich source of experimental information for hydrogen passivated shallow- and deep-level defects.

On the contrary, in oxide semiconductors, hydrogen has been predicted to be an important *source* of *n*-type conductivity.[99–104] Modern theory has drawn attention to work from the 1950s where hydrogen was found to give rise to shallow donors in ZnO,[105,106] and has predicted the properties of hydrogen shallow donors in several transparent conducting oxides.

Two defects have been predicted to be shallow donors in several oxide hosts: interstitial hydrogen, H_i, and hydrogen trapped at an oxygen vacancy, H_O.[99–104] H_i forms strong O-H bonds with stretching frequencies near 3500 cm^{-1}. H_O gives rise to an unusual multicenter bond with a much lower vibrational frequency that has made it challenging to study by vibrational spectroscopy. In ZnO, for example, H_O is predicted to be located at an oxygen vacancy surrounded by four Zn neighbors.[101] The calculated vibrational frequency is 760 cm^{-1}.

Hydrogen in ZnO gives rise to both H_i and H_O shallow donors whose properties have been investigated extensively by experiment. An O-H stretching line that is polarized along the c-axis of ZnO was found at 3611 cm^{-1} and the corresponding O-D line was found at 2668 cm^{-1} (Fig. 14).[107] The 3611 cm^{-1} line was found to be marginally stable at room temperature, and has been assigned to the H_i shallow donor.[108–110] (When H_i in ZnO is annealed away at temperatures near 150 °C, it forms the interstitial H_2 molecule,[92,93] which is discussed in Sec. IV E.[111,112]) ZnO also contains a more thermally stable hydrogen shallow donor[108–110] that theory predicted is due to H_O.[101]

The vibrational mode predicted for H_O in ZnO lies in a region where ZnO is strongly absorbing and is difficult to study.[101] In this case, photothermal-ionization spectroscopy (PTIS) was used to detect the vibrational modes of H_O.[112] In PTIS, Ohmic contacts are made to the front surface of the hydrogen-containing sample. A thin layer of the sample itself is then used as a photoconductive detector of the absorbed light, making it possible to measure spectra in a frequency range where the sample is highly absorbing.

The photoconductivity spectrum of a ZnO:H sample is shown in Fig. 15. The vibrational absorption lines at 742 and 792 cm^{-1} are seen as negative peaks in the spectrum.[112] The H_O center in ZnO has C_{3V} symmetry. The 742 cm^{-1} mode was found to be polarized parallel to the c-axis and was assigned to an A_1 mode of the defect. The 792 cm^{-1} mode was found to be polarized perpendicular to the c-axis, and was assigned to an E vibrational mode.

The vibrational spectra of the H_i center detected by conventional means,[107] and the H_O center detected by PTIS[112] provide detailed microscopic information about hydrogen shallow donors in ZnO and an excellent test of the predictions of theory.

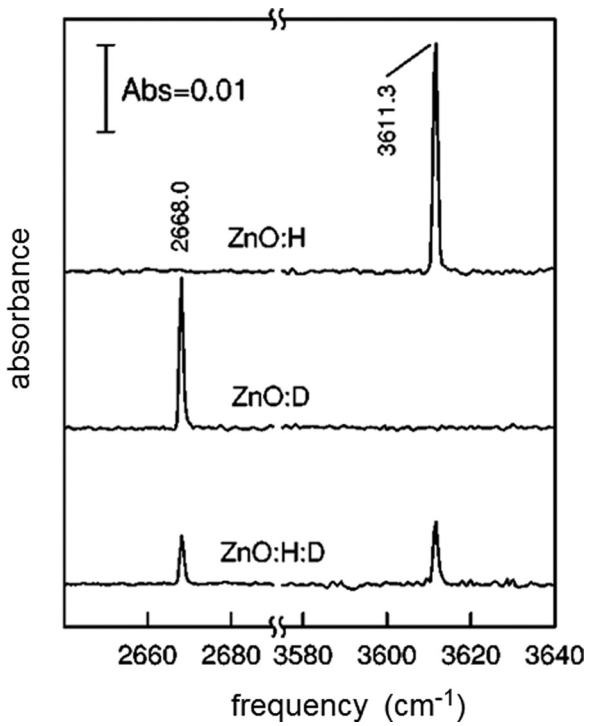

FIG. 14. Absorption spectra (10 K) of ZnO samples after treatments in H-, D- and (H + D)-containing plasmas. The absorption lines assigned to the H_i and D_i centers are shown. [Adapted with permission from Lavrov *et al.*, Phys. Rev. B **66**, 165205 (2002). Copyright 2002 American Physical Society.]

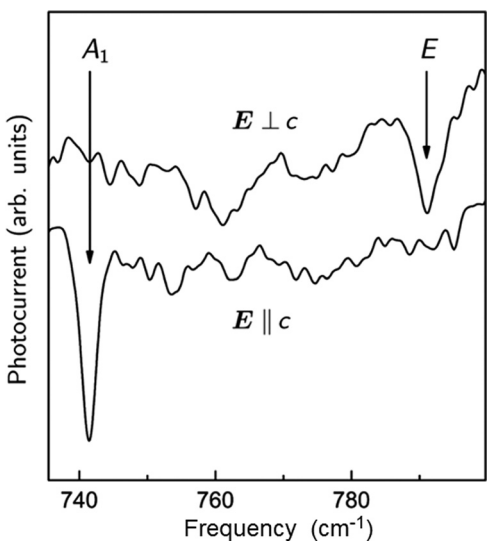

FIG. 15. Vibrational lines assigned to the H_O center in hydrogenated ZnO seen in a photoconductivity spectrum measured at 12 K. Polarization of the light with respect to the c axis is shown. [Reproduced with permission from Koch *et al.*, Phys. Rev. Lett. **108**, 165501 (2012). Copyright 2012 American Physical Society.]

B. OH-Li in ZnO

Investigations of the OH-Li center in ZnO bring together several facets of what can be learned about a defect from its vibrational properties and theory.

ZnO grown by the hydrothermal method shows a dominant OH vibrational line at 3577.3 cm^{-1} and a corresponding OD line at 2644.5 cm^{-1} (Fig. 16).[113–115] The solvent used for the hydrothermal growth of ZnO contains Li, so the 3577.3 cm^{-1} line was suggested to be due to a defect complex containing Li.

The vibrational spectra shown in Fig. 16 reveal the chemical composition of the OH-Li center.[116] (i) The isotope shift of the dominant IR line from 3577.3 to 2644.5 cm^{-1} upon the substitution of D for H establishes the presence of H in the OH-Li center. (ii) Weak satellite lines at 3571.7 and 3566.6 cm^{-1} with intensities consistent with the natural isotopic abundances of ^{16}O (99.759%), ^{17}O (0.037%), and ^{18}O (0.204%) show that H is bonded to oxygen. (iii) The OH line at 3577.3 cm^{-1} shows no additional structure when measured at high resolution. However, the OD line at 2644.5 cm^{-1} is narrower than its OH partner, presumably because the vibrational lifetime is greater for the OD-Li center than for OH-Li. The reduced vibrational line width for the OD-Li center reveals a weak shoulder at 2644.7 cm^{-1}. The relative intensities of the 2644.5 cm^{-1} line and its shoulder at 2644.7 cm^{-1} are consistent with the natural abundances of ^{7}Li (92.5%) and ^{6}Li (7.5%), unambiguously proving that Li is present in the defect complex.

The spectra shown in Fig. 16 also show the second harmonic modes at 6967 and 5191 cm^{-1} for the dominant ^{16}OH and ^{16}OD modes, respectively, allowing their anharmonicities to be determined.[116]

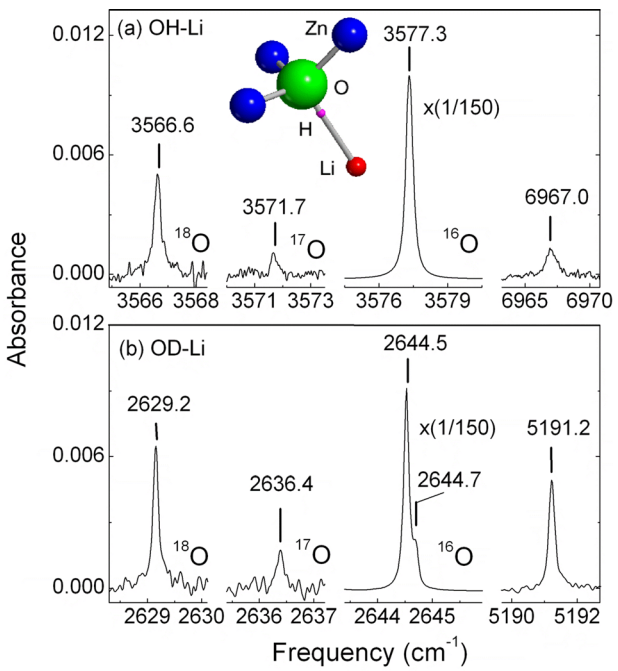

FIG. 16. Absorption spectra (4.2 K) for ZnO samples containing Li. The sample for the spectrum shown in (a) was annealed in H_2 gas and the sample shown in (b) was annealed in D_2 gas. The inset shows the structure of the OH-Li complex in ZnO. [Reproduced with permission from Shi *et al.*, Phys. Rev. B **73**, 081201 (2006). Copyright 2006 American Physical Society.]

There are three different structural models that could be consistent with the measured vibrational properties of the OH-Li center.[114] Theory completes the picture of the OH-Li center in ZnO by predicting that the structure shown in the inset in Fig. 16(a) has lowest energy.[116] The OH-Li center provides an excellent example of a defect whose structure and properties have been determined by the combined strengths of experiment and theory.

C. Small polaron characteristics of an OD center in TiO_2

The charge carriers in oxide semiconductors can be delocalized or can be self-trapped to form small polarons.[117] Of particular interest here are polarons that can be spatially localized in the vicinity of impurities in oxides.[118–122] Hydrogen bonded to oxygen in the rutile structure of TiO_2 has attracted recent interest because the extra electron contributed by the neutral charge state of H in rutile TiO_2 becomes self-trapped, and acts as a small polaron!

The vibrational properties of OH and OD centers in TiO_2, while studied for decades,[123] have recently revealed new surprises.[124,125] (The properties of OD are discussed here because its vibrational lines are sharper than those of OH, and revealed greater detail.) Early studies of the vibrational properties of the OD center in TiO_2 found a single sharp vibrational line at 2445.0 cm^{-1} [Fig. 17, spectrum (i)].[123] On the contrary, recent studies find a more complicated OD spectrum with a multiline structure with lines at 2445.0, 2445.7, and 2447.8 cm^{-1} [Fig. 17, spectrum (ii)].[124,125] It was recognized that the early studies of OD centers in TiO_2 focused on samples that had been fully oxygenated, resulting in a charged OD^+ center that gives a single sharp line. However, if samples are slightly reduced by annealing in a D_2 ambient, a neutral

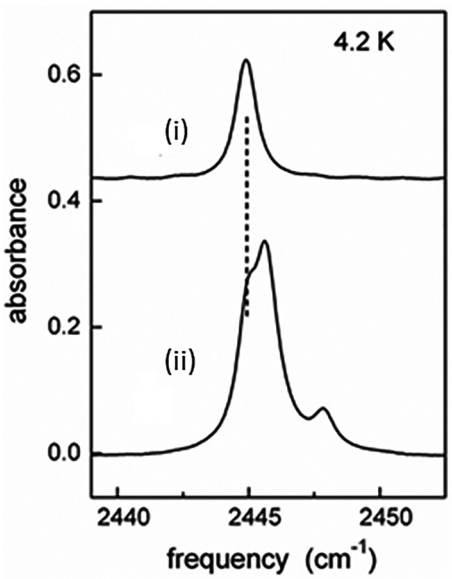

FIG. 17. Absorption spectra (4.2 K) for TiO_2 samples deuterated by annealing in a D_2 ambient. The sample for spectrum (ii) was measured without further annealing. The sample for spectrum (i) was annealed in air (30 min at 500 °C) to introduce additional oxygen. [Reproduced with permission from Bekisli *et al.*, Phys. Rev. B **86**, 155208 (2012). Copyright 2012 American Physical Society.]

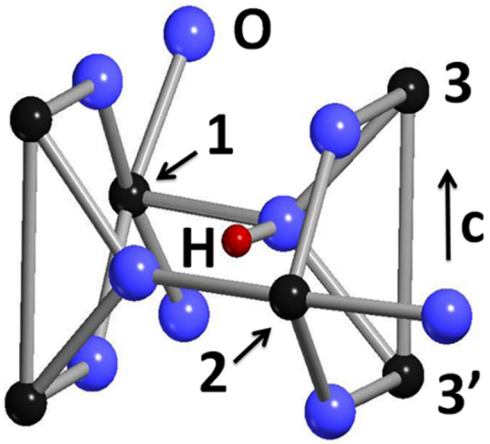

FIG. 18. The different configurations for the neutral OD center in TiO_2 with a negative charge localized on different Ti^{3+} neighbors. [Reproduced with permission from Bekisli *et al.*, Phys. Rev. B **86**, 155208 (2012). Copyright 2012 American Physical Society.]

OD^0 center with an extra electron is produced, which has the multiline structure that was observed recently.[124,125]

The multiline OD^0 vibrational spectrum has a strong dependence on temperature, which has been explored in detail. These experimental results and their interpretation by theory showed that the properties of the neutral OD^0 center in TiO_2 can be explained by a small polaron model, which involves several configurations in which the OD^0 center's extra electron becomes trapped at different nearby Ti sites (Fig. 18). Configurations with the electron localized at different Ti sites have different O-D vibrational frequencies, explaining the multiline spectrum. Each configuration has a slightly different ground-state energy so that the self-trapped electron may occupy different Ti sites when the temperature is changed.[125]

The interpretation of the vibrational spectrum of the OD center in TiO_2 and its temperature dependence in terms of a small polaron[125] is consistent with recent theory,[118–120] an EPR study of OH that finds the electron associated with the neutral center localized on a nearby Ti,[122] and muon spin resonance results.[126]

A recent study has found an additional O-H vibrational line near 3500 cm^{-1} in TiO_2 whose vibrational frequency is also shifted by the trapping of a small polaron at a nearby Ti site.[127]

D. The diffusivity of the interstitial hydrogen shallow-donor center in In_2O_3

Hydrogen has been predicted to be an *n*-type dopant in In_2O_3 that gives rise to unintentional conductivity.[103] Muon spin resonance experiments find that implanted muons, whose properties mimic those of hydrogen, also form shallow donors in In_2O_3.[128] Furthermore, hydrogen can be an intentional dopant, and has attracted attention for solar-cell applications.[129–131] The diffusivity of the H_i^+ center in In_2O_3 has been determined experimentally by complementary methods based on vibrational spectroscopy.[132] The structure of the hydrogen shallow donor and the mechanism for a diffusion jump have been predicted by theory.[133]

Annealing single-crystal samples of In_2O_3 in an H_2 ambient produces several O-H vibrational lines, in addition to the broad, low-frequency absorption that arises from free carriers.[134] In annealing experiments, the infrared (IR) absorption line observed at 3306 cm^{-1} was found to be correlated with the free-carrier absorption produced by hydrogen. Therefore, the 3306 cm^{-1} line was assigned to the interstitial H_i^+ center whose structure is shown in Fig. 19(a).

Two types of experiments have been performed to determine the diffusivity of H_i^+ in In_2O_3 from its IR absorption spectra[132]

(i) At temperatures near 700 K, the O-H line at 3306 cm^{-1} has been used to determine the diffusivity of H_i^+ from its indiffusion and outdiffusion behaviors. An In_2O_3 sample was annealed in an H_2 ambient to introduce hydrogen. The sample was thinned in steps, while the 3306 cm^{-1} line was monitored to determine the penetration depth of the H_i^+ center and, thereby, its diffusivity.

When a hydrogenated In_2O_3 sample is annealed in an inert N_2 ambient, the disappearance of the 3306 cm^{-1} line is governed by the outdiffusion of the H_i^+ center. An analysis of the outdiffusion behavior of H_i^+ with a model based on Fick's second law also yielded the diffusivity of H_i^+.

(ii) IR absorption experiments were performed in conjunction with stress to probe the symmetry and reorientation of the H_i^+ center. These experiments showed that the splitting of the 3306 cm^{-1} line produced by stress was consistent with C_{1h} symmetry, and with the structure predicted by theory.[133]

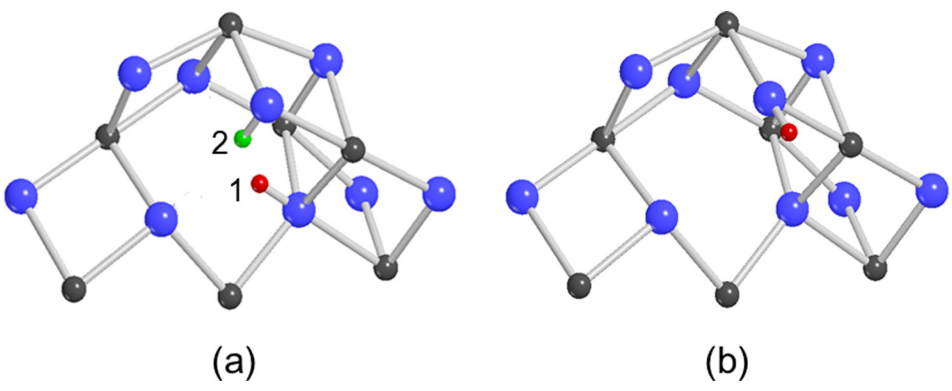

FIG. 19. Defect models showing the pathway for a diffusion jump of H_i^+ in In_2O_3. The lowest energy configuration (1) for H_i^+ is AB_{01} shown in (a). A metastable configuration (2), AB_{02} is predicted to lie 0.51 eV higher in energy. (b) shows a near-lying AB_{01} site.

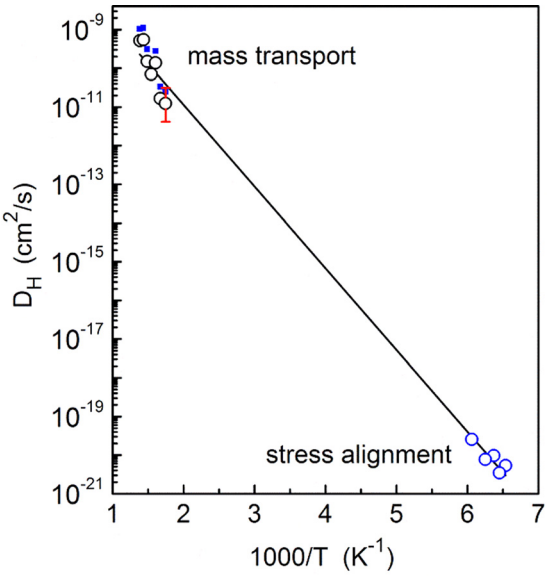

FIG. 20. The diffusivity vs. 1000/T for the interstitial hydrogen shallow donor center in In_2O_3. [Reproduced with permission from Qin *et al.*, J. Appl. Phys. **123**, 161506 (2018). Copyright 2018 American Institute of Physics.]

At temperatures near 160 K, stress was used to produce a preferential alignment of the H_i^+ center, which could be detected in IR absorption experiments made with polarized light. Furthermore, theory predicted that the process by which this alignment is produced is also a diffusion jump. This two-step diffusion-jump for H_i^+ in In_2O_3 is shown in Fig. 19. With the help of theory, the kinetics with which the stress-induced alignment was produced yielded the time constant for a single jump of the H_i^+ center, and also the diffusivity of H_i^+ near 160 K.[132,133]

The combination of the diffusivity of H_i^+ found near 698 K by mass-transport measurements along with the diffusivity found near 160 K from the time constant for a single H_i^+ jump determines the diffusivity for H_i^+ in In_2O_3 for over eleven orders of magnitude (Fig. 20)! These results are reminiscent of the determination of the diffusivity of interstitial oxygen in Si performed decades earlier (Sec. III B).

VI. CONCLUSION

A defect containing a light-mass element and its nearest neighbors can be identified from the shifts in its vibrational modes caused by the natural abundances of the isotopes making up the defect and by intentional isotopic substitutions. This tutorial includes a few examples where the atoms that make up a defect and their microscopic structure have been determined from the isotopic structure of the vibrational lines.

However, much can be learned from a defect's vibrational spectrum. There are a growing number of defects for which novel properties not obviously accessible from a defect's vibrational spectrum have been discovered, often with help of additional perturbations and complementary theory. Several examples have been chosen where the ability of vibrational spectroscopy to determine the properties of a defect surprises us. Furthermore, there will undoubtedly be new surprises for which the novel properties of defects will be revealed unexpectedly by their vibrational spectra.

ACKNOWLEDGMENTS

This work was partially supported by NSF Grant No. DMR 1160756. M.S. is grateful for the support and for the visits to Dresden from the Humboldt Foundation.

[1]*Identification of Defects in Semiconductors*, edited by M. Stavola (Academic Press, San Diego, 1998/1999), Vols. 51A and 51B.
[2]M. D. McCluskey and E. E. Haller, *Dopants and Defects in Semiconductors* (CRC Press, Boca Raton, 2012).
[3]B. Pajot, *Optical Absorption of Impurities and Defects in Semiconducting Crystals, I. Hydrogen-like Centres* (Springer-Verlag, Berlin, 2010).
[4]The proceedings of the first International Conference on Defects in Semiconductors was published as an issue of the J. Appl. Phys. titled, Conference on Radiation Effects in Semiconductors, J. Appl. Phys. **30**, 1117 (1959).
[5]B. Pajot and B. Clerjaud, *Optical Absorption of Impurities and Defects in Semiconducting Crystals. II. Electronic Absorption of Deep Centres and Vibrational Spectra* (Springer-Verlag, Berlin, 2013).
[6]R. C. Newman, *Infrared Studies of Crystal Defects* (Taylor and Francis, London, 1973).
[7]A. S. Barker and A. J. Sievers, Rev. Mod. Phys. **47**(Suppl. No. 2), S1–S179 (1975).
[8]R. Murray and R. C. Newman, in *Landolt-Börnstein, New Series*, edited by O. Madelung and M. Schulz (Springer-Verlag, Berlin, 1989), Vol. 22b.
[9]R. C. Newman, in *Imperfections in III-V Materials*, edited by E. Weber (Academic Press, Boston, 1993), p. 117.
[10]M. Stavola, *Identification of Defects in Semiconductors* (Academic Press, 1999), Ref. 1, Vol. 51B, p. 153.
[11]M. D. McCluskey, J. Appl. Phys. **87**, 3593 (2000).
[12]S. K. Estreicher, D. Backlund, T. M. Gibbons, and A. Doçaj, Modell. Simul. Mater. Sci. Eng. **17**, 084006 (2009).
[13]B. Prévot and J. Wagner, Prog. Cryst. Growth Charact. **22**, 245 (1991).
[14]H. Y. Fan, Rep. Prog. Phys. **19**, 107 (1956).
[15]P. R. Griffiths and J. A. de Haseth, *Fourier Transform Infrared Spectrometry* (Wiley-Interscience, New York, 1986).
[16]B. Pajot, Analusis **7**, 293 (1977).
[17]P. G. Dawber and R. J. Elliott, Proc. Phys. Soc. **81**, 453 (1963).
[18]J. Weber, M. Hiller, and E. V. Lavrov, Physica B **401–402**, 91 (2007).
[19]J. Wagner and M. Ramsteiner, IEEE J. Quantum Electron. **25**, 993 (1989).
[20]W. B. Fowler, R. Capelletti, and E. Colombi, Phys. Rev. B **44**, 2961 (1991).
[21]E. E. Haller, J. Appl. Phys. **77**, 2857 (1995).
[22]*Oxygen in Silicon*, edited by F. Shimura (Academic Press, Boston, 1994).
[23]W. Kaiser, P. H. Keck, and C. F. Lange, Phys. Rev. **101**, 1264 (1956).
[24]H. J. Hrostowski and R. H. Kaiser, Phys. Rev. **107**, 966 (1957).
[25]B. Pajot, *Oxygen in Silicon* (Academic Press, 1994), Ref. 22, p. 191.
[26]B. Pajot, E. Artacho, C. A. J. Ammerlaan, and J.-M. Spaeth, J. Phys.: Condens. Matter **7**, 7077 (1995).
[27]D. R. Bosomworth, W. Hayes, A. R. L. Spray, and G. D. Watkins, Proc. R. Soc. London A **317**, 33 (1970).
[28]H. Yamada-Kaneta, C. Kaneta, and T. Ogawa, Phys. Rev. B **42**, 9650 (1990).
[29]R. C. Newman, Semicond. Sci. Technol. **9**, 1749 (1994).
[30]O. G. Lorimor and W. G. Spitzer, J. Appl. Phys. **37**, 3687 (1966).
[31]W. M. Theis, K. K. Bajaj, C. W. Litton, and W. G. Spitzer, Appl. Phys. Lett. **41**, 70 (1982).
[32]R. C. Newman, F. Thompson, M. Hyliands, and R. F. Peart, Solid State Commun. **10**, 505 (1972).
[33]C. Freysoldt, B. Grabowski, T. Hickel, J. Neugebauer, G. Kresse, A. Jannotti, and C. G. Van de Walle, Rev. Mod. Phys. **86**, 253 (2014).
[34]G. Kresse and J. Furthmüller, Phys. Rev. B **54**, 11169 (1996).
[35]R. Dovesi, V. R. Saunders, C. Roetti, R. Orlando, C. M. Zicovich-Wilson, F. Pascale, B. Civalleri, K. Doll, N. M. Harrison, I. J. Bush, P. D'Arco, and M. Llunell, *Crystal06 User's Manual* (University of Torino, Torino, 2006).

[36]D. Sánchez-Portal, P. Ordejón, E. Artacho, and J. M. Soler, Int. J. Quantum. Chem. **65**, 453 (1997).
[37]R. Jones and P. R. Briddon, *Identification of Defects in Semiconductors* (Academic Press, 1988), Vol. 51A, Ref. 1, p. 288.
[38]R. Jones, J. Goss, C. Ewels, and S. Öberg, Phys. Rev. B **50**, 8378 (1994).
[39]S. Limpijumnong, J. E. Northrup, and C. G. Van de Walle, Phys. Rev. B **68**, 075206 (2003).
[40]A. R. Woll and W. B. Fowler, Phys. Rev. B **48**, 16788 (1993).
[41]M. G. Weinstein, M. Stavola, K. L. Stavola, S. J. Uftring, J. Weber, J.-U. Sachse, and H. Lemke, "An example of defects that show different line frequencies when their charge states are changed are the PtH_n complexes in Si," Phys. Rev. B **65**, 035206 (2001).
[42]M. Stavola, S. J. Pearton, J. Lopata, C. R. Abernathy, and K. Bergman, "Stress experiments that combined stress splittings to determine defect symmetry and stress alignment to probe defect motion were performed for the Be-H complex in GaAs," Phys. Rev. B **39**, 8051 (1989).
[43]A. A. Kaplyanskii, Opt. Spectrosc. **16**, 329 (1964).
[44]J. A. Wolk, M. B. Kruger, J. N. Heyman, W. Walukiewicz, R. Jeanloz, and E. E. Haller, Phys. Rev. Lett. **66**, 774 (1991).
[45]M. D. McCluskey and E. E. Haller, Phys. Rev. B **56**, 9520 (1997).
[46]G. Lüpke, N. H. Tolk, and L. C. Feldman, J. Appl. Phys. **93**, 2317 (2003).
[47]D. West and S. K. Estreicher, Phys. Rev. B **75**, 075206 (2007).
[48]M. Budde, C. Parks Cheney, N. H. Tolk, and L. C. Feldman, Phys. Rev. Lett. **85**, 1452 (2000).
[49]B. Bech Nielsen, L. Hoffman, and M. Budde, Mater. Sci. Eng. **36**, 259 (1996).
[50]M. Budde, B. Bech Nielsen, P. Leary, J. Goss, R. Jones, P. R. Briddon, S. Öberg, and S. J. Breuer, Phys. Rev. B **57**, 4397 (1998).
[51]M. Suezawa, Phys. Rev. B **63**, 035201 (2000).
[52]M. Budde, G. Lüpke, E. Chen, X. Zhang, N. H. Tolk, L. C. Feldman, E. Tarhan, A. K. Ramdas, and M. Stavola, Phys. Rev. Lett. **87**, 145501 (2001).
[53]J. D. Holbech, B. Bech Nielsen, R. Jones, P. Sitch, and S. Öberg, Phys. Rev. Lett. 71, 875 (1993).
[54]G. Lüpke, X. Xhang, B. Sun, A. Fraser, N. H. Tolk, and L. Feldman, Phys. Rev. Lett. **88**, 135501 (2002).
[55]B. Sun, G. A. Shi, S. V. S. Nageswara Rao, M. Stavola, N. H. Tolk, S. K. Dixit, L. C. Feldman, and G. Lüpke, Phys. Rev. Lett. **96**, 035501 (2006).
[56]K. K. Kohli, G. Davies, N. Q. Vinh, D. West, S. K. Estreicher, T. Gregorkiewicz, I. Izeddin, and K. M. Itoh, Phys. Rev. Lett. **96**, 225503 (2006).
[57]T. M. Gibbons, S. K. Estreicher, K. Potter, F. Bekisli, and M. Stavola, Phys. Rev. B **87**, 115207 (2013).
[58]J. W. Corbett, R. S. McDonald, and G. D. Watkins, J. Phys. Chem. Solids **25**, 873 (1964).
[59]M. Stavola, J. R. Patel, L. C. Kimerling, and P. E. Freeland, Appl. Phys. Lett. **42**, 73 (1983).
[60]R. C. Newman, J. H. Tucker, and F. M. Livingston, J. Phys. C: Solid State Phys. **16**, L151 (1983).
[61]J. C. Mikkelsen, Appl. Phys. Lett. **40**, 336 (1982).
[62]G. D. Watkins, J. W. Corbett, and R. S. McDonald, J. Appl. Phys. **53**, 7097 (1982).
[63]R. C. Newman and R. Jones, *Oxygen in Silicon* (Academic Press, 1994), Ref. 21.
[64]D. V. Lang and R. A. Logan, Phys. Rev. Lett. **39**, 635 (1977).
[65]D. V. Lang, R. A. Logan, and M. Jaros, Phys. Rev. B **19**, 1015 (1979).
[66]P. M. Mooney, J. Appl. Phys. **67**, R1 (1990).
[67]D. J. Chadi and K. J. Chang, Phys. Rev. Lett. **61**, 873 (1988).
[68]D. J. Chadi and K. J. Chang, Phys. Rev. B **39**, 10063 (1989).
[69]M. Saito, A. Oshiyama, and O. Sugino, Phys. Rev. B **45**, 13745 (1992).
[70]J. Schneider, B. Dischler, H. Seelewind, P. M. Mooney, J. Lagowski, M. Matsui, D. R. Beard, and R. C. Newman, Appl. Phys. Lett. **54**, 1442 (1989).
[71]H. C. Alt, Phys. Rev. Lett. **65**, 3421 (1990).
[72]M. Skowronski, S. T. Neild, and R. E. Kremer, Appl. Phys. Lett. **57**, 902 (1990).
[73]G. D. Watkins and J. W. Corbett, Phys. Rev. **121**, 1001 (1961).
[74]R. Jones and S. Öberg, Phys. Rev. Lett. **69**, 136 (1992).
[75]R. Eisberg and R. Resnick, *Quantum Physics of Atoms, Molecules, Solids, Nuceli and Particles*, 2nd ed. (Wiley, New York, 1985).
[76]A. Mainwood and A. M. Stoneham, Physica **116B**, 101 (1983).
[77]J. W. Corbett, S. N. Sahu, T. S. Shi, and L. C. Snyder, Phys. Lett. A **93**, 303 (1983).
[78]J. Vetterhöffer, J. Wagner, and J. Weber, Phys. Rev. Lett. **77**, 5409 (1996).
[79]M. Stavola, E. E. Chen, W. B. Fowler, and G. A. Shi, Physica B **340–342**, 58 (2003).
[80]A. W. R. Leitch, V. Alex, and J. Weber, Phys. Rev. Lett. **81**, 421 (1998).
[81]R. E. Pritchard, M. J. Ashwin, J. H. Tucker, and R. C. Newman, Phys. Rev. B **57**, 15048 (1998).
[82]E. E. Chen, M. Stavola, W. B. Fowler, and P. Walters, Phys. Rev. Lett. **88**, 105507 (2002).
[83]W. B. Fowler, P. Walters, and M. Stavola, Phys. Rev. B **66**, 075216 (2002).
[84]G. A. Shi, M. Stavola, W. B. Fowler, and E. E. Chen, Phys. Rev. B **72**, 085207 (2005).
[85]E. V. Lavrov and J. Weber, Phys. Rev. Lett. **89**, 215501 (2002).
[86]M. Hiller, E. V. Lavrov, and J. Weber, Phys. Rev. Lett. **98**, 055504 (2007).
[87]C. Peng, M. Stavola, W. B. Fowler, and M. Lockwood, Phys. Rev. B **80**, 125207 (2009).
[88]V. P. Markevich and M. Suezawa, J. Appl. Phys. **83**, 2988 (1998).
[89]E. E. Chen, M. Stavola, and W. B. Fowler, Phys. Rev. B **65**, 245208 (2002).
[90]M. Hiller, E. V. Lavrov, and J. Weber, Physica B **401**, 97 (2007).
[91]M. Hiller, E. V. Lavrov, J. Weber, B. Hourahine, R. Jones, and P. R. Briddon, Phys. Rev. B **72**, 153201 (2005).
[92]E. V. Lavrov, F. Herklotz, and J. Weber, Phys. Rev. Lett. **102**, 185502 (2009).
[93]S. G. Koch, E. V. Lavrov, and J. Weber, Phys. Rev. B **90**, 205212 (2014).
[94]*Oxide Semiconductors*, edited by B. G. Svensson, S. J. Pearton, and C. Jagadish (Academic Press, Amsterdam, 2013).
[95]P. D. C. King and T. D. Veal, J. Phys.: Condens. Matter **23**, 334214 (2011).
[96]J. L. Lyons, A. Janotti, and C. G. Van de Walle, *Oxide Semiconductors* (Academic Press, 2013), Ref. 94, p. 1.
[97]M. D. McCluskey, M. C. Tarun, and S. T. Teklemichael, J. Mater. Res. **27**, 2190 (2012).
[98]S. J. Pearton, J. W. Corbett, and M. Stavola, *Hydrogen in Crystalline Semiconductors* (Springer-Verlag, Heidelberg, 1992).
[99]C. G. Van de Walle, Phys. Rev. Lett. **85**, 1012 (2000).
[100]C. Kiliç and A. Zunger, Appl. Phys. Lett. **81**, 73 (2002).
[101]A. Janotti and C. G. Van de Walle, Nat. Mater. **6**, 44 (2007).
[102]A. K. Singh, A. Janotti, M. Scheffler, and C. G. Van de Walle, Phys. Rev. Lett. **101**, 055502 (2008).
[103]S. Limpijumnong, P. Reunchan, A. Janotti, and C. G. Van de Walle, Phys. Rev. B **80**, 193202 (2009).
[104]J. B. Varley, J. R. Weber, A. Janotti, and C. G. Van de Walle, Appl. Phys. Lett. **97**, 142106 (2010).
[105]G. Heiland, E. Mollwo, and F. Stöckman, in *Solid State Physics*, edited by F. Seitz and D. Turnbull (Academic Press, New York, 1959), Vol. 8, p. 193.
[106]D. G. Thomas and J. J. Lander, J. Chem. Phys. **25**, 1136 (1956).
[107]E. V. Lavrov, J. Weber, F. Börrnert, C. G. Van de Walle, and R. Helbig, Phys. Rev. B **66**, 165205 (2002).
[108]G. A. Shi, M. Stavola, S. J. Pearton, M. Thieme, E. V. Lavrov, and J. Weber, Phys. Rev. B **72**, 195211 (2005).
[109]E. V. Lavrov, F. Herklotz, and J. Weber, Phys. Rev. B **79**, 165210 (2009).
[110]S. G. Koch, E. V. Lavrov, and J. Weber, Phys. Rev. B **89**, 235203 (2014).
[111]G. Shi, M. Saboktakin, M. Stavola, and S. J. Pearton, Appl. Phys. Lett. **85**, 5601 (2004).
[112]S. G. Koch, E. V. Lavrov, and J. Weber, Phys. Rev. Lett. **108**, 165501 (2012).
[113]C. H. Seager and S. M. Myers, J. Appl. Phys. **94**, 2888 (2003).
[114]L. E. Halliburton, L. Wang, L. Bai, N. Y. Garces, N. C. Giles, M. J. Callahan, and B. Wang, J. Appl. Phys. **96**, 7168 (2004).
[115]E. V. Lavrov, F. Börrnert, and J. Weber, Phys. Rev. B **71**, 035205 (2005).
[116]G. A. Shi, M. Stavola, and W. B. Fowler, Phys. Rev. B **73**, 081201 (2006).
[117]D. Emin, *Polarons* (Cambridge University Press, Cambridge, 2012).
[118]J. Stausholm-Møller, H. H. Kristoffersen, B. Hinnemann, G. K. H. Madsen, and B. Hammer, J. Chem. Phys. **133**, 144708 (2010).
[119]P. Deák, B. Aradi, and T. Frauenheim, Phys. Rev. B **83**, 155207 (2011).
[120]A. Janotti, C. Franchini, J. B. Barley, G. Kresse, and C. G. Van de Walle, Phys. Status Solidi RRL **7**, 199 (2013).
[121]S. Yang and L. E. Halliburton, Phys. Rev. B **81**, 035204 (2010).

[122]A. T. Brant, S. Yang, N. C. Giles, and L. E. Halliburton, J. Appl. Phys. **110**, 053714 (2011).
[123]J. B. Bates and R. A. Perkins, Phys. Rev. B **16**, 3713 (1977).
[124]F. Herklotz, E. V. Lavrov, and J. Weber, Phys. Rev. B **83**, 235202 (2011).
[125]F. Bekisli, W. B. Fowler, and M. Stavola, Phys. Rev. B **86**, 155208 (2012).
[126]R. C. Vilão, R. B. L. Vieira, H. V. Alberto, J. M. Gil, A. Weidinger, R. L. Lichti, B. B. Baker, P. W. Mengyan, and J. S. Lord, Phys. Rev. B **92**, 081202 (2015).
[127]A. Hupfer, L. Vines, E. V. Monakhov, and B. G. Svensson, Phys. Rev. B **96**, 085203 (2017).
[128]P. D. C. King, R. L. Lichti, Y. G. Celebi, J. M. Gil, R. C. Vilão, H. V. Alberto, J. Piroto Duarte, D. J. Payne, R. G. Egdell, I. McKenzie, C. F. McConville, S. F. J. Cox, and T. D. Veal, Phys. Rev. B **80**, 081201(R) (2009).
[129]T. Koida, H. Fujiwara, and M. Kondo, Jpn. J. Appl. Phys. **46**, L685 (2007).
[130]T. Koida, H. Sai, and M. Kondo, Thin Solid Films **518**, 2930 (2010).
[131]B. Macco, M. S. Verheijen, L. E. Black, B. Barcones, J. Melskens, and W. M. M. Kessels, J. Appl. Phys. **120**, 085314 (2016).
[132]Y. Qin, P. Weiser, K. Villalta, M. Stavola, W. B. Fowler, I. Biaggio, and L. Boatner, J. Appl. Phys. **123**, 161506 (2018).
[133]P. Weiser, Y. Qin, W. Yin, M. Stavola, W. B. Fowler, and L. A. Boatner, Appl. Phys. Lett. **109**, 202105 (2016).
[134]W. Yin, K. Smithe, P. Weiser, M. Stavola, W. B. Fowler, L. A. Boatner, S. J. Pearton, D. C. Hays, and S. Koch, Phys. Rev. B **91**, 075208 (2015).